APPLIED GEOPHYSICS, Vol.18, No.3 (September 2021), P. 317–330, 14 Figures.
DOI:10.1007/s11770-021-0901-7

An improved convolution perfectly matched layer for elastic second-order wave equation*

Yang Ling-Yun[1,2], Wu Guo-Chen♦[1,2], Li Qing-Yang[1,2], and Liang Zhan-Yuan[1,2]

Abstract: A convolution perfectly matched layer (CPML) can efficiently absorb boundary reflection in numerical simulation. However, the CPML is suitable for the first-order elastic wave equation and is difficult to apply directly to the second-order elastic wave equation. In view of this, based on the first-order CPML absorbing boundary condition, we propose a new CPML (NCPML) boundary which can be directly applied to the second-order wave equation. We first systematically extend the first-order CPML technique into second-order wave equations, neglecting the space-varying characteristics of the partial damping coefficient in the complex-frequency domain, avoiding the generation of convolution in the time domain. We then transform the technique back to the time domain through the inverse Fourier transform. Numerical simulation indicates that the space-varying characteristics of the attenuation factor have little influence on the absorption effect and increase the memory at the same time. A number of numerical examples show that the NCPML proposed in this study is effective in simulating elastic wave propagation, and this algorithm is more efficient and requires less memory allocation than the conventional PML absorbing boundary.
Keywords: Convolutional perfectly matched layer; absorbing boundary conditions; second-order elastic wave equation; numerical simulation

Introduction

Since the actual medium in the underground is unbounded, artificial boundaries have to be established by numerical simulation, resulting in that the problem of artificial boundary reflection will inevitably occur. To eliminate boundary reflections in the computational domain, numerous absorbing boundary conditions (ABCs) have been developed (Clayton and Engquist, 1977, Reynolds, 1978, Cerjan et al., 1985, Lian and Zhang, 2013).

Berenger (1994) proposed a new ABC based on the Maxwell equation: the PML absorption boundary. The classical PML is formulated from complex coordinate stretching (CCS) Chew and Weedon, 1994). Collino and Tsogka (2001) applied this boundary to the numerical simulation of the first-order elastic wave equation. However, CCS has a drawback in handling grazing and evanescent waves. Kuzuogulu and Mittra (1996) proposed a complex frequency shift (CFS-PML) that can attenuate grazing waves. The CFS-PML boundary condition requires the introduction of too many auxiliary variables, leading to expensive computation (Berenger, 2002). Roden and Gedney (2000) proposed convolution PML (CPML) boundary conditions using recursive

Manuscript received by the Editor May 5, 2020; revised manuscript received June 15, 2021..
*This work was supported by the National Science and Technology Major Special Sub-project of China (No. 2016ZX05024-001-008) and the National Natural Science Foundation Joint Fund Project of China (No. U1562215).
1 School of Geosciences, China University of Petroleum (East China), Qingdao 266580, Shandong, China
2 Laboratory for Marine Mineral Resources, Qingdao National Laboratory for Marine Science and Technology, Qingdao 266071, Shandong, China.
♦Corresponding author: Wu Guochen (Email: guochenwu@upc.edu.cn).

methods. Komatitsch (2007) used this method to solve the first-order velocity–stress elastic wave equation. For the numerical simulation method of the second-order isotropic and anisotropic acoustic wave equation, Drossaert and Giannopoulos (2007) proposed the Recursive Integral-PM (RI-PML), which calculates integrals instead of convolution; Sun (2019) extended it to mesh-free finite difference scheme. At present, the PML absorption boundary has been widely applied in the numerical simulation of porous elastic media (Martin et al., 2008a), anisotropic media (Becache et al., 2003, Martin et al., 2008b; Pasalic and McGarry, 2010), and viscoelastic media (Martin and Komatitsch, 2009).

In the past, this PML was mainly used for first-order systems, and there are few studies on PML for second-order systems. In order to apply the PML absorption boundary to the second-order elastic wave equation, Komatitsch and Trompt (2003) first introduce the PML to the second-order elastic wave equation. Xing (2006) applied this method to the acoustic wave equation by converting a second-order equation into a first-order equation. Although this method is effective, it requires more computational storage. Pinton et al. (2012) proposed a PML absorption boundary for the acoustic wave equation without splitting the wavefield. However, the method involves deconvolution. At present, the first- and second-order PMLs of the acoustic wave equation have been widely used in numerical simulation: The first-order PML has been studied, whereas research about the second-order PML is few.

Inspired by the first-order CPML equation, we use the iterative format instead of convolution to construct second-order new CPML (NCPML) boundary conditions. We first review the conventional second-order splitting PML (SPML) and CPML boundary elastic wave equation deduce the second-order NCPML boundary elastic wave equation, theoretically proving the validity of the method. Following that, we use homogeneous media to prove that the varying characteristics of the partial damping coefficient have little effect on the absorption effect and require more memory. Then, we use a layer model to compare the SPML, CPML, and NCPML boundaries to show that NCPML has more advantages in improving the computation storage and computing the efficiency and absorption effect. Finally, we use a Marmousi-2 model to illustrate the stability of the NCPML absorption boundary to the complex medium model.

Second-order NCPML boundary

There are two conventional forms of the PML absorption boundary: splitting and unsplitting. The conventional SPML needs to split the wavefield, which increases the number of equations and the computational storage, and the absorption effect for grazing waves is less efficient. The unsplitting CPML not only fixes the disadvantages of the conventional PML but also needs less memory and computes efficiently. Unfortunately, the conventional CPML boundary is formulated as a first-order system in velocity and stress, which means that it cannot be directly applied to a second-order system in displacement. This paper combines the CPML's absorption properties at grazing incidence and the idea of reducing memory by neglecting attenuation factor spatiality and proposes the NCPML boundary.

The displacement–stress elastic wave equation is as follows (Virieux, 1986):

$$\begin{cases} \rho \dfrac{\partial^2 u_x}{\partial t^2} = \dfrac{\partial \sigma_{xx}}{\partial x} + \dfrac{\partial \tau_{xz}}{\partial z} \\ \rho \dfrac{\partial^2 u_z}{\partial t^2} = \dfrac{\partial \tau_{xz}}{\partial x} + \dfrac{\partial \sigma_{zz}}{\partial z} \\ \sigma_{xx} = (\lambda + 2\mu)\dfrac{\partial u_x}{\partial x} + \lambda \dfrac{\partial u_z}{\partial z} + f_x \\ \sigma_{zz} = (\lambda + 2\mu)\dfrac{\partial u_z}{\partial z} + \lambda \dfrac{\partial u_x}{\partial x} + f_z \\ \tau_{xz} = \mu\left(\dfrac{\partial u_x}{\partial z} + \dfrac{\partial u_z}{\partial x}\right) + f_{xz} \end{cases}, \tag{1}$$

where σ_{xx} and σ_{zz} are normal stress, τ_{xz} presents shear stress, λ and μ are lame constants, ρ is the density of the medium, μ_x and μ_z represent the displacement wavefields in the horizontal and vertical directions, respectively, and f_x, f_z, and f_{xz} are the source terms.

Eliminating the stress components in equation (1), the corresponding second-order elastic wave equation in homogeneous media (ignoring the source terms) is

$$\begin{cases} \rho \dfrac{\partial^2 u_x}{\partial t^2} = (\lambda + 2\mu)\dfrac{\partial^2 u_x}{\partial x^2} + \mu \dfrac{\partial^2 u_x}{\partial z^2} \\ \qquad\qquad + (\lambda + \mu)\dfrac{\partial^2 u_z}{\partial x \partial z} \\ \rho \dfrac{\partial^2 u_z}{\partial t^2} = \mu \dfrac{\partial^2 u_z}{\partial x^2} + (\lambda + 2\mu)\dfrac{\partial^2 u_z}{\partial z^2} \\ \qquad\qquad + (\lambda + \mu)\dfrac{\partial^2 u_x}{\partial x \partial z} \end{cases}. \tag{2}$$

The frequency-domain form is (Yin et al., 2006)

$$\begin{cases} (i\omega)^2 \rho \hat{u}_x = (\lambda+2\mu)\dfrac{\partial^2 \hat{u}_x}{\partial x^2} + \mu \dfrac{\partial^2 \hat{u}_x}{\partial z^2} \\ \qquad\qquad + (\lambda+\mu)\dfrac{\partial^2 \hat{u}_z}{\partial x \partial z} \\ (i\omega)^2 \rho \hat{u}_z = \mu \dfrac{\partial^2 \hat{u}_z}{\partial x^2} + (\lambda+2\mu)\dfrac{\partial^2 \hat{u}_z}{\partial z^2} \\ \qquad\qquad + (\lambda+\mu)\dfrac{\partial^2 \hat{u}_x}{\partial x \partial z} \end{cases}, \tag{3}$$

where $\hat{u}_x$ and $\hat{u}_z$ represents the frequency-domain wavefield.

The complex stretching variable of CPML absorbing boundaries (Roden and Gedney, 2000) in the x-axis is

$$\begin{cases} \partial_{\tilde{x}} = \dfrac{1}{s_x}\dfrac{\partial}{\partial x} \\ s_x = k_x(x) + \dfrac{d_x(x)}{\alpha_x(x) + i\omega} \end{cases}, \tag{4}$$

where $i = \sqrt{-1}$, $d_x(x)$ represents the damping profile in the traditional PML that attenuates the transmission wave, and $a_x(x)$, $b_x(x)$ represent the complex frequency shift and the grid compression parameter, respectively. In the computational domain, k_x=1 and d_x=0. The specific application parameters can be seen in Appendix B.

Substituting equation (4) into equation (3), the following equation is obtained:

$$\begin{cases} (i\omega)^2 \hat{u}_x = v_p^2 \dfrac{1}{s_x}\dfrac{\partial}{\partial x}\left(\dfrac{1}{s_x}\dfrac{\partial \hat{u}_x}{\partial x}\right) \\ \qquad + v_s^2 \dfrac{1}{s_z}\dfrac{\partial}{\partial z}\left(\dfrac{1}{s_z}\dfrac{\partial \hat{u}_x}{\partial z}\right) \\ \qquad + \left(v_p^2 - v_s^2\right)\dfrac{1}{s_x}\dfrac{\partial}{\partial x}\left(\dfrac{1}{s_z}\dfrac{\partial \hat{u}_z}{\partial z}\right) \\ (i\omega)^2 \hat{u}_z = v_p^2 \dfrac{1}{s_z}\dfrac{\partial}{\partial z}\left(\dfrac{1}{s_z}\dfrac{\partial \hat{u}_z}{\partial z}\right) \\ \qquad + v_s^2 \dfrac{1}{s_x}\dfrac{\partial}{\partial x}\left(\dfrac{1}{s_x}\dfrac{\partial \hat{u}_z}{\partial x}\right) \\ \qquad + \left(v_p^2 - v_s^2\right)\dfrac{1}{s_x}\dfrac{\partial}{\partial x}\left(\dfrac{1}{s_z}\dfrac{\partial \hat{u}_x}{\partial z}\right) \end{cases}, \tag{5}$$

where v_p and v_s are the P- and S-wave velocities, respectively, with $v_p = \sqrt{\dfrac{\lambda+2\mu}{\rho}}$ and $v_s = \sqrt{\dfrac{\mu}{\rho}}$.

Taking directly the inverse Fourier transform of the stretching variable in equation (5) will be too complex. Taking $\partial_{\tilde{x}^2}$ and $\partial_{\tilde{x}\tilde{z}}$ as an example

$$\begin{cases} \partial_{\tilde{x}^2} = F^{-1}\left(\dfrac{1}{s_x^2}\right) * \dfrac{\partial^2}{\partial x^2} \\ \qquad + F^{-1}\left(\dfrac{1}{s_x}\right) * F^{-1}\left(\dfrac{\partial}{\partial x}\left(\dfrac{1}{s_x}\right)\right) * \dfrac{\partial}{\partial x} \\ \partial_{\tilde{x}\tilde{z}} = F^{-1}\left(\dfrac{1}{s_x s_z}\right) * \dfrac{\partial^2}{\partial x \partial z} \\ \qquad + F^{-1}\left(\dfrac{1}{s_x}\right) * F^{-1}\left(\dfrac{\partial}{\partial x}\left(\dfrac{1}{s_z}\right)\right) * \dfrac{\partial}{\partial z} \end{cases}, \tag{6}$$

where F^{-1} represents the inverse Fourier transform and * is the convolution operator.

In order to avoid the generation of convolution terms in the time domain, the spatial variation properties of the damping coefficient $1/s_x$ and $1/s_z$ are ignored; then, equation (6) can be simplified as

$$\begin{cases} \partial_{\tilde{x}^2} = F^{-1}\left(\dfrac{1}{s_x^2}\right) * \dfrac{\partial^2}{\partial x^2} \\ \partial_{\tilde{x}\tilde{z}} = F^{-1}\left(\dfrac{1}{s_x s_z}\right) * \dfrac{\partial^2}{\partial x \partial z} \end{cases}. \tag{7}$$

Substituting equation (4) into equation (7), the following is obtained:

$$\begin{cases} \dfrac{1}{s_x s_x} = \dfrac{1}{(k_x)^2} - \dfrac{2d_x}{k_x^3}\dfrac{1}{(d_x/k_x+\alpha_x)+i\omega} + \dfrac{d_x^2}{k_x^4}\dfrac{1}{\left((d_x/k_x+\alpha_x)+i\omega\right)^2} \\ \dfrac{1}{s_x s_z} = \left(\begin{array}{l} \dfrac{1}{k_x k_z} - \dfrac{d_x}{k_z k_x^2}\dfrac{1}{(d_x/k_x+\alpha_x)+i\omega} \\ - \dfrac{d_z}{k_x k_z^2}\dfrac{1}{(d_z/k_z+\alpha_z)+i\omega} \\ + \dfrac{d_x d_z}{k_x^2 k_z^2}\dfrac{1}{\left((d_x/k_x+\alpha_x)+i\omega\right)\left((d_z/k_z+\alpha_z)+i\omega\right)} \end{array}\right) \end{cases}. \tag{8}$$

Noting that the Fourier transform of $\delta(t)$ is 1 and the Fourier transform of $e^{-at}H(t)$ is $1/(a+i\omega)$, $\bar{s}_x^2$ and $\bar{s}_{x,z}$ are denoted as the inverse Fourier transform of $\dfrac{1}{s_x s_x}$

and $\dfrac{1}{s_x s_z}$:

$$\begin{cases} \overline{s}_x^2 = \dfrac{\delta(t)}{(k_x)^2} - \dfrac{2d_x}{k_x^3} H(t) e^{-(d_x/k_x+\alpha_x)t} \\ \quad + \dfrac{d_x^2}{k_x^4} H(t) e^{-(d_x/k_x+\alpha_x)t} * H(t) e^{-(d_x/k_x+\alpha_x)t} \\ \overline{s}_{x,z} = \left(\begin{array}{l} \dfrac{\delta(t)}{k_x k_z} - \dfrac{d_x}{k_z k_x^2} H(t) e^{-(d_x/k_x+\alpha_x)t} - \dfrac{d_z}{k_x k_z^2} H(t) e^{-(d_z/k_z+\alpha_z)t} \\ + \dfrac{d_x d_z}{k_x^2 k_z^2} H(t) e^{-(d_x/k_x+\alpha_x)t} * H(t) e^{-(d_z/k_z+\alpha_z)t} \end{array} \right) \end{cases}, \tag{9}$$

where $\delta(t)$ denotes the Dirac delta and $H(t)$ denotes the Heaviside distributions.

We denote

$$\xi_x(t) = -\frac{d_x}{k_x^2} H(t) e^{-(d_x/k_x+\alpha_x)t}. \tag{10}$$

(1) When $d_x/k_x + a_x \neq d_z/k_z + a_z$, then equation (9) will become

$$\begin{cases} \partial_{\tilde{x}^2} = \dfrac{\partial_{x^2}}{(k_x)^2} + \dfrac{2}{k_x} \xi_x(t) * \partial_{x^2} - \dfrac{d_x}{k_x^2} t \xi_x(t) * \partial_{x^2} \\ \partial_{\tilde{x}\tilde{z}} = \left(\begin{array}{l} \dfrac{\partial_{xz}}{k_x k_z} + \left(\dfrac{1}{k_z} \xi_x(t) + \dfrac{1}{k_x} \xi_z(t) \right) * \partial_{xz} \\ + \dfrac{d_z}{k_z^2} \dfrac{\xi_x(t)}{d_x/k_x + \alpha_x - d_z/k_z - \alpha_z} * \partial_{xz} \\ - \dfrac{d_x}{k_x^2} \dfrac{\xi_z(t)}{d_x/k_x + \alpha_x - d_z/k_z - \alpha_z} * \partial_{xz} \end{array} \right) \end{cases}. \tag{11}$$

The convolution term is computed at time step n, the time interval is Δt, and we denote

$$\psi_x^n = \left(\xi_x(t) * \frac{\partial^2}{\partial x^2} \right)^n = \int_0^{n\Delta t} \left(\frac{\partial^2}{\partial x^2} \right)^{n\Delta t - \tau} \xi_x(\tau) d\tau = \sum_{m=0}^{n-1} \left(\frac{\partial^2}{\partial x^2} \right)^{n-\left(m-\frac{1}{2}\right)} Z_x(m), \tag{12}$$

and

$$\psi_{x,1}^n = \left(\xi_x(t) * \frac{\partial^2}{\partial x \partial z} \right)^n = \int_0^{n\Delta t} \left(\frac{\partial^2}{\partial x \partial z} \right)^{n\Delta t - \tau} \xi_x(\tau) d\tau = \sum_{m=0}^{n-1} \left(\frac{\partial^2}{\partial x \partial z} \right)^{n-\left(m-\frac{1}{2}\right)} Z_x(m), \tag{13}$$

with

$$Z_x(m) = \int_{m\Delta t}^{(m+1)\Delta t} \xi_x(\tau) d\tau. \tag{14}$$

If we denote

$$\begin{cases} b_x = e^{-(d_x/k_x+\alpha_x)m\Delta t} \\ a_x = \dfrac{d_x}{k_x(d_x/k_x+\alpha_x)} \left(b_x - 1 \right) \end{cases}, \tag{15}$$

then

$$Z_x(m) = a_x e^{-(d_x/k_x+\alpha_x)dt}. \tag{16}$$

Because of the exponential form of equation (16), equations (12) and (13) can be written in recursive form

$$\begin{cases} \psi_x^n - b_x \psi_x^{n-1} = a_x \left(\partial_{x^2} \right)^{n-\frac{1}{2}} \\ \psi_{x,1}^n - b_x \psi_{x,1}^{n-1} = a_x \left(\partial_x \partial_z \right)^{n-\frac{1}{2}} \end{cases}. \tag{17}$$

Substituting equation (17) into equation (11), we obtain

$$\begin{cases} \partial_{\tilde{x}^2} = \dfrac{\partial_{x^2}}{(k_x)^2} + \dfrac{2}{k_x} \psi_x^n - \dfrac{d_x}{k_x^2} t \psi_x^n \\ \partial_{\tilde{x}\tilde{z}} = \dfrac{\partial_{xz}}{k_x k_z} \left(\begin{array}{l} + \left(\dfrac{1}{k_z} - \dfrac{d_z}{k_z^2} \dfrac{1}{d_z/k_z + \alpha_z - d_x/k_x - \alpha_x} \right) \psi_{x,1}^n \\ + \left(\dfrac{1}{k_x} - \dfrac{d_x}{k_x^2} \dfrac{1}{d_x/k_x + \alpha_x - d_z/k_z - \alpha_z} \right) \psi_{z,1}^n \end{array} \right) \end{cases}, \tag{18}$$

and update ψ_x^n, $\psi_{x,1}^n$, and $\psi_{z,1}^n$ in the time domain according to equation (17).

Finally, substituting equation (18) into equation (2), the second-order elastic wave equation with the NCPML boundary is obtained

$$\begin{cases} \dfrac{\partial^2 u}{\partial t^2} = \begin{vmatrix} v_p^2\left(\dfrac{1}{(k_x)^2}\dfrac{\partial^2 u}{\partial x^2}+\left(\dfrac{2}{k_x}-\dfrac{d_x}{k_x^2}t\right)\psi^n_{u,x}\right)+v_s^2\left(\dfrac{1}{(k_z)^2}\dfrac{\partial^2 u}{\partial z^2}+\left(\dfrac{2}{k_z}-\dfrac{d_z}{k_z^2}t\right)\psi^n_{u,z}\right) \\ +\left(v_p^2-v_s^2\right)\left(\dfrac{1}{k_xk_z}\dfrac{\partial^2\omega}{\partial x\partial z}+\begin{pmatrix}\left(\dfrac{1}{k_z}-\dfrac{d_z}{k_z^2}\dfrac{1}{d_z/k_z+\alpha_z-d_x/k_x-\alpha_x}\right)\psi^n_{\omega,x,1} \\ +\left(\dfrac{1}{k_x}-\dfrac{d_x}{k_x^2}\dfrac{1}{d_x/k_x+\alpha_x-d_z/k_z-\alpha_z}\right)\psi^n_{\omega,z,1}\end{pmatrix}\right) \end{vmatrix} \\ \dfrac{\partial^2\omega}{\partial t^2} = \begin{vmatrix} v_s^2\left(\dfrac{1}{(k_x)^2}\dfrac{\partial^2\omega}{\partial x^2}+\left(\dfrac{2}{k_x}-\dfrac{d_x}{k_x^2}t\right)\psi^n_{\omega,x}\right)+v_p^2\left(\dfrac{1}{(k_z)^2}\dfrac{\partial^2\omega}{\partial z^2}+\left(\dfrac{2}{k_z}-\dfrac{d_z}{k_z^2}t\right)\psi^n_{\omega,z}\right) \\ +\left(v_p^2-v_s^2\right)\left(\dfrac{1}{k_xk_z}\dfrac{\partial^2 u}{\partial x\partial z}+\begin{pmatrix}\left(\dfrac{1}{k_z}-\dfrac{d_z}{k_z^2}\dfrac{1}{d_z/k_z+\alpha_z-d_x/k_x-\alpha_x}\right)\psi^n_{u,x,1} \\ +\left(\dfrac{1}{k_x}-\dfrac{d_x}{k_x^2}\dfrac{1}{d_x/k_x+\alpha_x-d_z/k_z-\alpha_z}\right)\psi^n_{u,z,1}\end{pmatrix}\right) \end{vmatrix} \end{cases} \tag{19}$$

(2) When $d_x / k_x + a_x = d_z / k_z + a_z$, the second-order elastic wave equation with the NCPML ABC is

$$\begin{cases} \dfrac{\partial^2 u}{\partial t^2} = \begin{vmatrix} v_p^2\left(\dfrac{1}{(k_x)^2}\dfrac{\partial^2 u}{\partial x^2}+\left(\dfrac{2}{k_x}-\dfrac{d_x}{k_x^2}t\right)\psi^n_{u,x}\right)+v_s^2\left(\dfrac{1}{(k_z)^2}\dfrac{\partial^2 u}{\partial z^2}+\left(\dfrac{2}{k_z}-\dfrac{d_z}{k_z^2}t\right)\psi^n_{u,z}\right) \\ +\left(v_p^2-v_s^2\right)\left(\dfrac{1}{k_xk_z}\dfrac{\partial^2\omega}{\partial x\partial z}+\left(\dfrac{1}{k_z}-\dfrac{td_z}{k_z^2}\right)\psi^n_{\omega,x,1}+\dfrac{1}{k_x}\psi^n_{\omega,z,1}\right) \end{vmatrix} \\ \dfrac{\partial^2\omega}{\partial t^2} = \begin{vmatrix} v_s^2\left(\dfrac{1}{(k_x)^2}\dfrac{\partial^2\omega}{\partial x^2}+\left(\dfrac{2}{k_x}-\dfrac{d_x}{k_x^2}t\right)\psi^n_{\omega,x}\right)+v_p^2\left(\dfrac{1}{(k_z)^2}\dfrac{\partial^2\omega}{\partial z^2}+\left(\dfrac{2}{k_z}-\dfrac{d_z}{k_z^2}t\right)\psi^n_{\omega,z}\right) \\ +\left(v_p^2-v_s^2\right)\left(\dfrac{1}{k_xk_z}\dfrac{\partial^2 u}{\partial x\partial z}+\left(\dfrac{1}{k_z}-\dfrac{td_z}{k_z^2}\right)\psi^n_{u,x,1}+\left(\dfrac{1}{k_x}\right)\psi^n_{u,z,1}\right) \end{vmatrix} \end{cases} \tag{20}$$

Numerical examples

To analyze the absorption effect and the stability of the NCPML boundary, the outline of the analysis process is as follows.

(1) First, the space-varying characteristics of the attenuation factor influencing the absorption effect and storage memory are analyzed.

(2) The advantages of the NCPML over the SPML boundary in terms of absorption effect, efficiency, and memory occupation are proved by a layered model, and the stability of NCPML for a complex model is verified by a Marmousi-2 model.

(3) Finally, by comparing the computational efficiencies of NCPML, CPML, and SPML, the advantages of NCPML in computational efficiency are obvious.

Analysis of the spatial variation of the attenuation factor

The second-order NCPML boundary proposed in this paper ignores the spatial variation of the attenuation factor and neglects the second part of the following equation:

$$\partial_{\tilde{x}^2} = \frac{1}{s_x^2}\partial_{x^2} + \frac{1}{s_x}\partial_x\left(\frac{1}{s_x}\right)\partial_x \approx \frac{1}{s_x^2}\partial_{x^2}. \tag{21}$$

To test the effects of the spatial variation of the attenuation factor, we take a homogeneous medium model with a size of 2000 × 2000 m to test the CPML boundary (denoted as CPML) and the NCPML boundary (denoted as NCPML). Table 1 shows a statistical table of the memory allocation and computational efficiency of the two boundaries. It shows that the storage memory and time required by the NCPML boundary are less than those of the CPML boundary. Therefore, the NCPML absorption boundary proposed in this paper neglects the spatial variation of the damping coefficient, sacrificing some absorption effect, but requires less storage memory and improves the efficiency.

Table 1. Statistical table of computational CPU time and memory allocation (1 MiB = 1,048,576 bytes)

Method	Computed time (s)	Required storage (MiB)
CPML	92.274	2.74
NCPML	73.015	2.13

Figs. 1a and 1c show the horizontal components of CPML and NCPML at 530 ms, respectively, and Figs. 1b and d shows the vertical components of CPML and NCPML at 530 ms, respectively. It can be seen from the figure that both boundaries have good absorption of the reflected waves, and there is no obvious reflection at the boundaries. In order to quantitatively analyze the absorption effect of the two absorbing boundaries, Figs. 2a and 3a show the comparison of the horizontal and vertical component values obtained by numerical simulation of the two PML boundaries at the dotted line (on the vertical line of x = 1000 m) in figure 1. Figs. 2b and 3b show the comparison of different absorption boundaries and theoretical values in the horizontal and vertical components. The theoretical value is calculated by adding the calculation domain; then, the calculated results are equal to the total absorbed at the boundary. We can see that the error of the horizontal component of

the wavefield of the CPML absorption boundary is 10^{-4} and the error of the vertical component is 10^{-6}, so the difference between the two boundaries can be ignored.

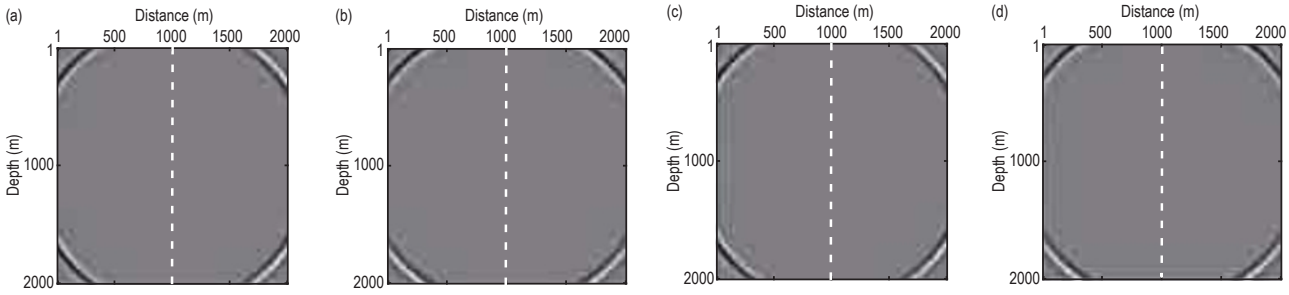

Figure 1. Wavefield snapshot at 530 ms under different absorption boundary conditions: (a) CPML boundary (horizontal component), (b) CPML boundary (vertical component), (c) NCPML boundary (horizontal component), and (d) NCPML boundary (vertical component).

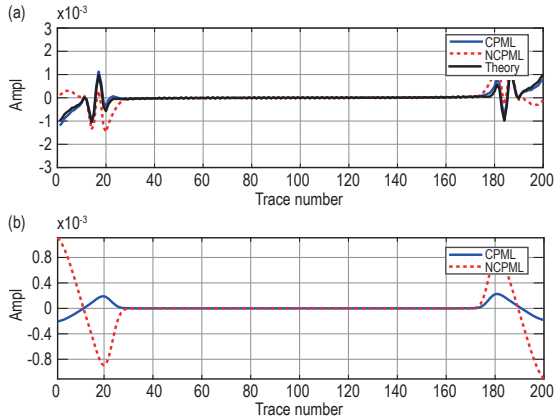

Figure 2. Waveforms computed by different absorption boundaries at position (1000 m, 0 m) (horizontal component): (a) Waveforms computed by different absorption boundaries at 530 ms and (b) amplitude deviation between theoretical value and that computed by different CPML boundary conditions at 530 ms.

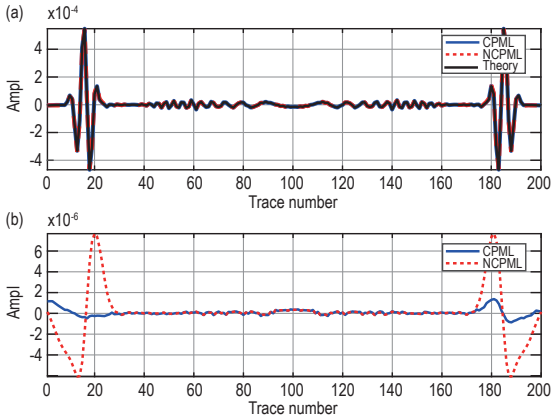

Figure 3. Waveforms computed by different absorption boundaries at position (1000 m, 0 m) (horizontal component): (a) Waveforms computed by different absorption boundaries at 530 ms and (b) amplitude deviation between theoretical value and that computed by different CPML boundary conditions at 530 ms.

In order to verify the stability of the NCPML absorption boundary. Figure 4 shows the total energy changes in the calculation area at different times. It can be seen that when the time is short, the absorption boundary does not play a role, so the energy of the three boundaries is the same. When the wave propagates to the boundary, it can be clearly seen that the energy of the SPML absorption boundary is stronger and the energy of the NCPML and CPML absorption boundaries is smaller. Figure. 5 verifies the characteristics of the wavefield at a large angle when the seismic source is placed on the surface. It can also be seen that SPML has obvious large-angle reflection, and both NCPML and CPML have good absorption effects on large-angle incident waves, which correspond to the previously proven absorption effects of the three absorption boundaries.

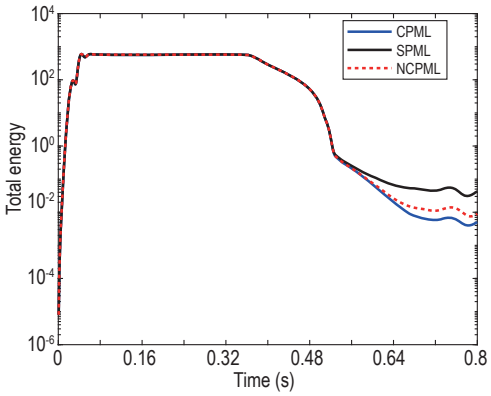

Figure 4. Total energy by different absorption boundaries.

Layer model

Numerical simulation of a four-layer model is carried out to verify the appropriateness and stability of the NCPML boundary. The grid size is 200 × 200, the spatial sampling interval is 10 m, the PML boundary is a 40-layer width, and the time sampling interval is 0.8 ms. The source's main frequency is a 25-Hz Ricker wavelet. The source is at coordinates (1000 m, 0 m). The geophone is arranged on the surface, and the velocity is shown in Figure 6.

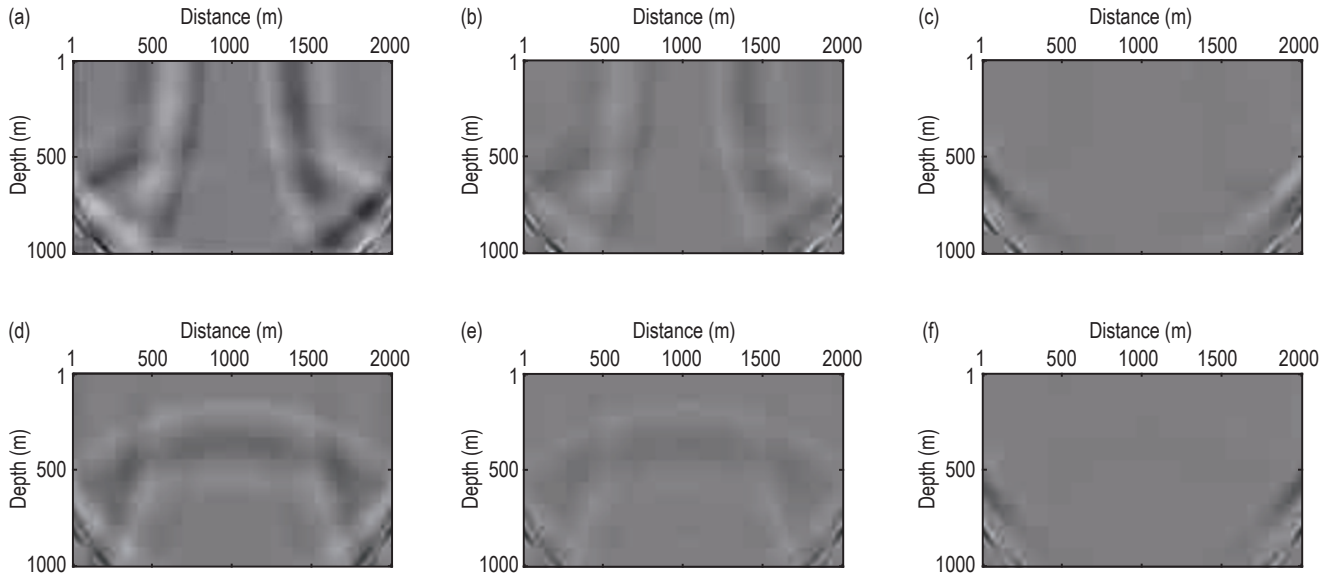

Figure 5. Wavefield snapshot at 800 ms under different absorption boundary conditions: (a) SPML boundary (horizontal component), (b) NCPML boundary (horizontal component), (c) CPML boundary (horizontal component), (d) SPML boundary (vertical component), (e) NCPML boundary (vertical component), and (f) CPML boundary (vertical component).

Figs. 7(a)–(f) presents the horizontal and vertical components of the SPML, NCPML, and CPML boundaries, respectively, at a time of 550 ms. There is almost no reflection of the artificial boundary at the wavefield boundary after loading the SPML and NCPML absorbing boundaries. It is clear that the SPML, NCPML, and CPML boundaries have good absorption effects on the reflected wave generated by the artificial boundary.

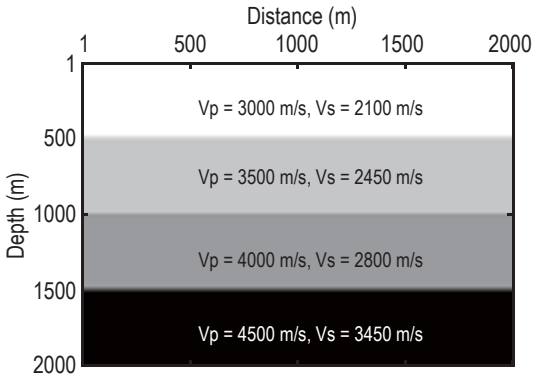

Figure 6. Velocity of the layered model.

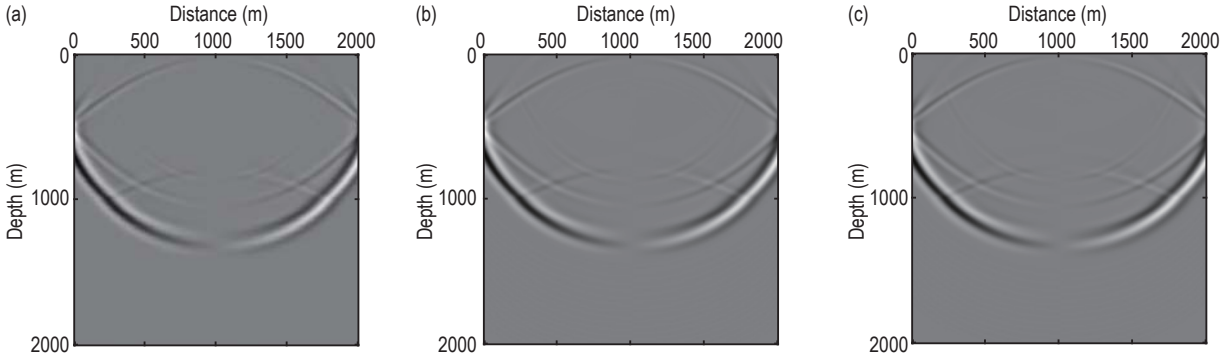

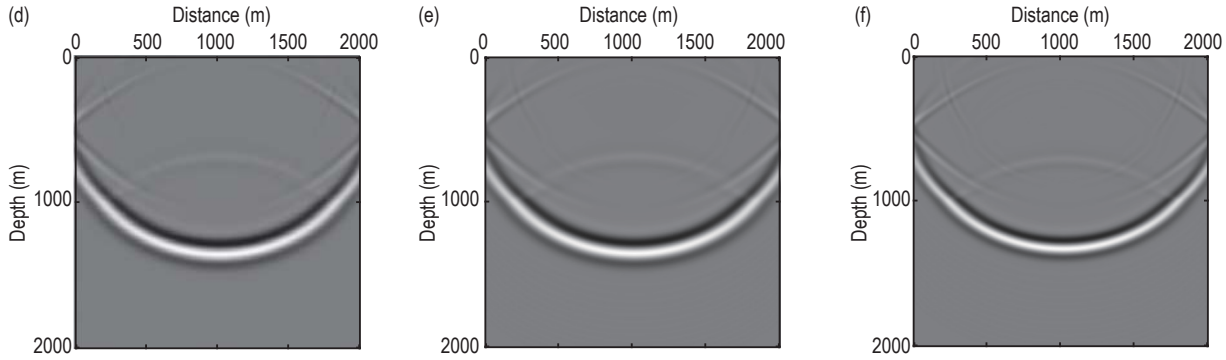

Figure 7. Wavefield snapshot at 550 ms under different methods of the layer model: (a) SPML boundary (horizontal component), (b) NCPML boundary (horizontal component), (c) CPML boundary (horizontal component), (d) SPML boundary (vertical component), (e) NCPML boundary (vertical component), and (f) CPML boundary (vertical component).

In order to quantitatively analyze the absorption effect of the absorbing boundary, Figs. 8a and 8b show the waveform curves of the 100th and 150th channels, respectively. Figure 9 shows the waveform part of Figure 8; we can see that the amplitude of the reflected wave under NCPML is not as good as that under CPML but better than that under the SPML boundary.

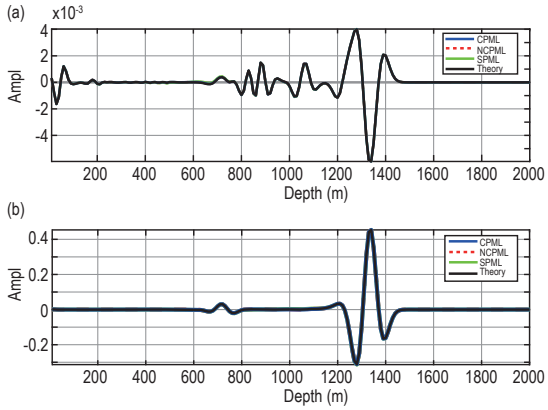

Figure 8. Horizontal component waveform of the layered model: (a) trace 10 and (b) trace 150 (the red line is the NCPML boundary, the green line is the NCPML boundary, the blue line is the CPML boundary, and the black line is the theory).

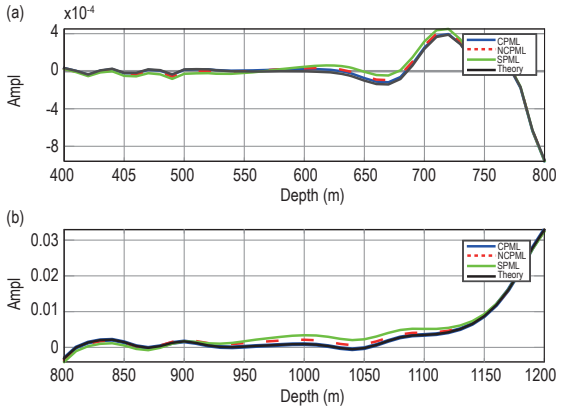

Figure 9. Comparison of seismic waveforms by different boundaries of the layered model at x = 1000 m (partial display): (a) horizontal component and (b) vertical component.

Figs. 10a and 10b show the horizontal and vertical component amplitude deviations between the theoretical values and the boundary wavefield for channel 100, respectively. Compared with the CPML boundary, NCPML has some shortages, but it has higher accuracy and is closer to the theoretical value than the SPML boundary.

Figs. 11a and 12a show the comparison of the numerical solutions and theoretical values of the seismic records at geophone points (500 m, 0 m) simulated by the SPML, CPML, and NCPML boundaries, respectively. The theoretical values are calculated by extending the calculation area, and the results

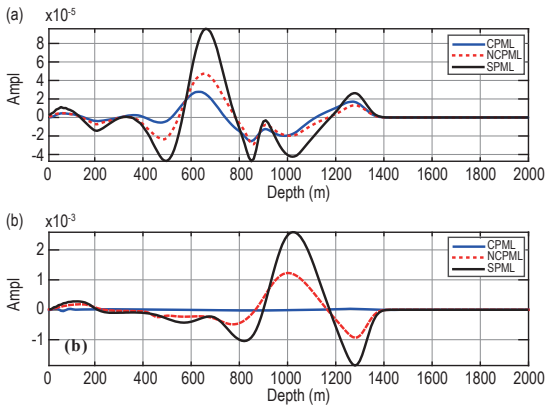

Figure 10. Amplitude deviation between theoretical values and different PML boundaries: (a) horizontal component and (b) vertical component.

are equivalent to the total absorbed. Generally, the calculated results of the three absorption boundaries are very close to the theoretical values. Fig. 11b shows a local enlargement of Fig. 11a (0.70–0.75 s), and Fig. 12b shows a local enlargement of Fig. 12a (0.1–0.25 s). The simulation results show that the CPML and NCPML boundaries basically coincide with the theoretical values, but the SPML absorption boundary has some errors, and the waveform amplitude is high. To quantitatively analyze their errors more intuitively, the SPML, CPML, and NCPML wavefields are compared with the theoretical ones. As shown in Fig. 12c, the maximum error of the SPML simulations is 2.5×10^{-3}, whereas that of CPML and NCPML is only 1.2×10^{-3}. In Fig. 10c, the maximum error of the SPML simulations is 8×10^{-3}, whereas that of the CPML and NCPML simulations is only 4×10^{-3}, which is about 50% of that of SPML. Therefore, the absorption effect of the NCPML boundary is better than that of the SPML boundary.

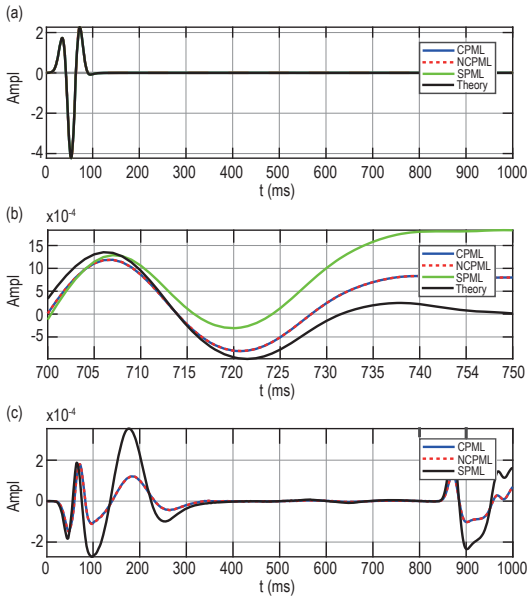

Figure 11. Horizontal component seismic records of the layered model for displacements at (500 m, 0 m): (a) Comparison of numerical solutions of seismic records, (b) numerical records of seismic records (partial display), and (c) different absorption boundaries with theoretical values.

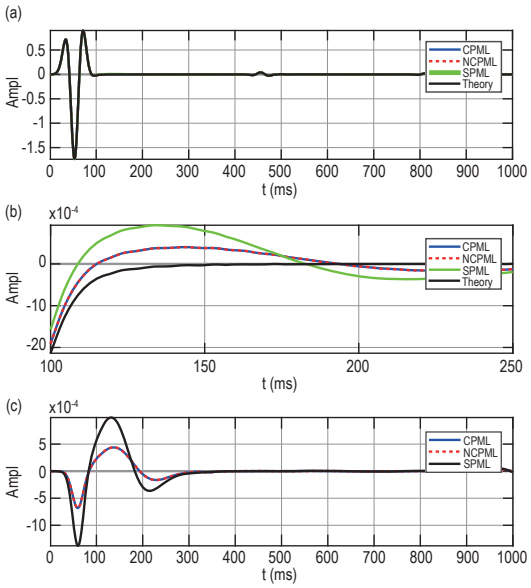

Figure 12. Vertical component seismic records of the layered model for displacements at (500 m, 0 m): Comparison of (a) numerical solutions of seismic records, (b) numerical records of seismic records (partial display), and (c) different absorption boundaries with theoretical values.

Marmousi-2 model

To further verify the suitability and stability of the NCPML boundary for the complex model, the complex Marmousi-2 model is used. As shown in Figure 13, the size of the model is 8000 m × 2000 m, the space step is 5 m, the main frequency is a 20-Hz Ricker wavelet, and the time interval is 0.4 ms. The excitation location of the source is sitting. The geophone is arranged on the surface, and the source is at the coordinates (4000 m, 0 m).

Fig. 14a and 14b shows the horizontal and vertical components recorded by the second-order NCPML absorbing boundary ground single gun, respectively. We can see from the observation that there is no obvious false reflection wave in the seismic records obtained by two different absorption boundaries. In order to highlight the reflection of the lower layer, an amplitude enhancement method is used to show it, which proves that the method is stable for the numerical simulation of

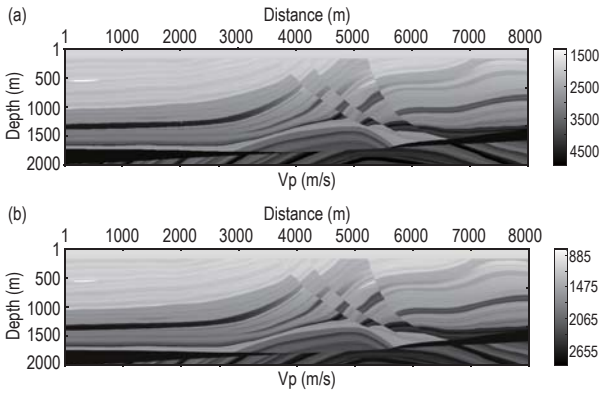

Figure 13. Velocity of the Marmousi-2 model.

complex models.

Comparison of calculation efficiencies

Compared with the second-order SPML absorbing boundary, the second-order NCPML absorbing boundary has the advantage of memory optimization; meanwhile, the computational efficiency can be greatly improved. Table 2 shows the memory and efficiency analysis of the different absorbing boundary algorithms on the same computer. The test models are the layered and Marmousi-2 models. In the testing process, I/O is not considered, and we only record the forward modeling time.

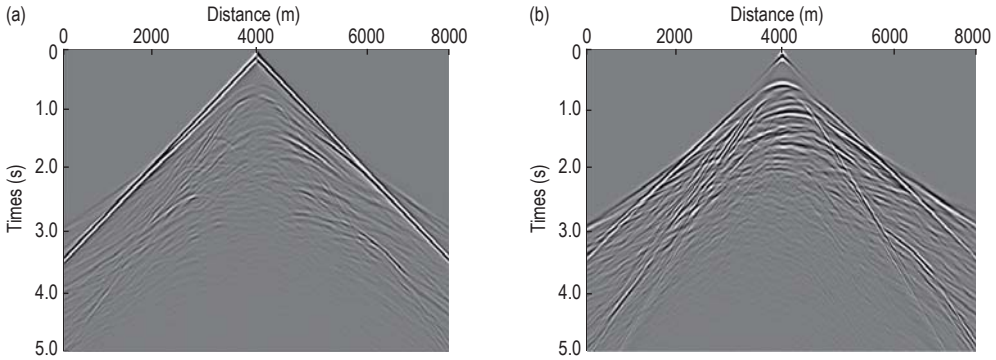

Figure 14. Seismic records for the Marmousi-2 model activated by one shot: (a) horizontal component and (b) vertical component.

Table 2. Statistical table of computational CPU time and memory allocation

Method	Layer model computed time (s)	Marmousi-2 model computed time (s)	Required storage
SPML	109.349	1503.774	20 arrays
CPML	95.529	1378.028	18 arrays
NCPML	79.944	1246.999	14 arrays

From the table above, the calculation speed of the second-order NCPML absorbing boundary deduced in this paper is faster than that of the second-order SPML boundary. When the model is small, the difference between them is not obvious. However, when the complexity of the model and the total computing time increase, the advantages of the NCPML absorbing boundary in terms of computing speed and memory can be obvious. In particular, when testing a three-dimensional model, the CPML absorbing boundary needs 66 three-dimensional arrays, whereas the SPML absorbing boundary needs 36 three-dimensional arrays. NCPML occupies about 50% of the SPML memory. The advantages of the NCPML absorbing boundary in terms of computing efficiency and memory optimization will be more obvious.

Conclusions

In this paper, a second-order elastic wave equation NCPML absorbing boundary is proposed. By ignoring the spatial variation of the damping coefficient in the complex-frequency domain, the generation of complex convolution in the time domain can be avoided, and the NCPML boundary is then transformed back to the time domain through the inverse Fourier transform. Finally, the second-order elastic wave equations based on the NCPML boundary were obtained and then applied to the second-order elastic wave numerical forward simulation. Numerical simulation shows that the NCPML boundary has good validity and stability. The following understandings are obtained through algorithm analysis and model test.

(1) First, the NCPML boundary elastic wave equation is systematically introduced. Through mathematical proof and layered model test, the NCPML, CPML, and SPML boundaries can efficiently absorb boundary reflection, and the NCPML absorption effect is better than that of SPML. Then, the stability of the proposed method is proved by the Marmousi-2 model.

(2) By analyzing the spatial variation of the damping

coefficient, the NCPML deduced in this paper neglects the spatial variation of the damping coefficient, sacrificing some absorption effect but saving storage memory and improving the computation efficiency.

(3) The numerical simulation results show that the NCPML absorbing boundary has great advantages in terms of memory. For the same two-dimensional model, the memory usage of the NCPML boundary is 30% less than that of the SPML boundary. When the model is extended to three-dimensional, the memory and accuracy advantages are more obvious, with the NCPML memory nearly 50% of that of the SPML boundary.

Acknowledgments

Thank two anonymous reviewers for their valuable comments on the revision of this article.

References

Becache, E., Fauqueux, S., and Joly, P., 2003, Stability of perfectly matched layers, group velocities and anisotropic waves: Journal of Computational Physics, **188**(2), 399−433.

Berenger, P. J., 1994, A perfectly matched layer for absorption of electromagnetic waves: Physics of Plasmas, **2**(114), 185−200.

Berenger, P. J., 2002, Numercial reflection from FDTD-PMLs: A comparison of the split PML with the unsplit and CFS PMLs: IEEE Transactions on Antennas and Propagation, **50**(3), 258−265.

Cerjan, C., Kosloff, D., and Kosloff, R., 1985, A nonreflecting boundary condition for discrete acoustic and elastic wave equations: Geophysics, **50**(4), 705−708.

Chew, W. C., and Weedon, H. W., 1994, A 3D perfectly matched medium from modified maxwell's equations with stretched coordinates: Microwave and Optical Technology Letters, **13**(7), 599−604.

Clayton, R., and Engquist, B., 1977, Absorbing boundary conditions for acoustic and elastic wave equations: Bulletin of the Seismological Society of America, **67**(6), 1529−1540.

Collino, F., and Tsogka, C., 2001, Application of the perfectly matched absorbing layer model to the linear elastodynamic problem in anisotropic heterogeneous media: Geophysics, **66**(1), 599−604.

Drossaert, F. H., and Giannopoulos, A., 2007, A nonsplit complex frequency-shifted PML based on recursive integration for FDTD modeling of elastic waves: Geophysics, **72**(2), T9−T17.

Festa, G., and Nielsen, S., 2003, PML absorbing boundaries: Bulletin of the Seismological Society of America, **93**(2), 891−903.

Katsibas, T. K., and Antonopulos, C. S., 2004, A general form of perfectly matched layers for three-dimensional problems of acoustic scattering in lossless and lossy fliuid media: Ultrasonics Ferroelectrics & Frequency Control IEEE Transactions on, **51**(8), 927−976.

Komatitsch, D., and Trompt, J., 2003, A perfectly matched layer absorbing boundary condition for the second-order seismic wave equation: Geophysical Journal International, **154**(1), 153−465.

Komatitsch, D., and Martin, R., 2007, An unsplit convolutional perfectly matched layer improved at grazing incidence for the seismic wave equation: Geophysics, **72**(5), M155−M167.

Kuzuogulu, M., and Mittra, R., 1996, Frequency dependence of the constitve paraments of causual perfectly matched anisotropic absorbers: IEEE Microwave and Guided wave letters, **6**(12), 447−449.

Li, Y. F., LI, G. F., and Wang, Y., 2010, Application of convolution perfectly matched layer in finite element method calculation for 2D acoustic wave: Acta Acustica, **35**(6), 601−607.

Lian, X. M., and Zhang, R. X., 2013, Numerical simulation of seismic wave equation by local discontinuous Galerkin method: Chinese Journal of Geophysics (in Chinese), **56**(10), 3507−3513.

Martin, R., and Komatitsch, D., 2009, An unsplit convolutional perfectly matched layer technique improved at grazing incidence for the viscoelastic wave equation: Geophysical Journal International, **179**(1), 333−344.

Martin, R., Komatitsch, D., and Ezziani, A., 2008, A variational formulation of a stabilized unsplit convolutional perfectly matched layer for the isotropic or anisotropic seismic wave equation: Computer Modeling in Engineering & Sciences, **37**(3), 274−304.

Martin, R., Komatitsch, D., and Ezziani, A., 2008, An unsplit convolutional perfectly matched layer improved at grazing incidence for seismic wave propagation in poroelastic media: Geophysics, **73**(4), T51−T61.

Pasalic D., and McGarry R., 2010, Convolutional

perfectly matched layer for isotropic and anisotropic acoustic wave equations: 80th Ann. Internat. Mtg, Soc. Expl. Geophys., Expanded Abstracts, 2925−2929.

Pinton, G. F., Dahl, J. and Rosenzweig, S., et al., 2012, A heterogeneous nonlinear attenuation full wave model of ultrasound: Ultrasonics Ferroelectrics & Frequency Control IEEE Transactions on, **56**(3), 1479−1485.

Qin, Z., Lu, M. H., Zheng, X. D., et al., 2009, The implementation of an improved NPML absorbing boundary condition in elastic wave modeling: Applied Geophysics, **6**(2), 113−121.

Reynolds, C. A., 1978, Boundary conditions for the numerical solution of wave propagation problems: Geophysics, **6**(43), 1099−1110.

Roden, A. J., and Gedney, D. S., 2000, Convolution PML (CPML): An efficient FDTD implementation of the CFS-PML for arbitrary media: Microwave and Optical Technology Letters, **27**(5), 334−339.

Sun, C. Y., Li, S. Z., and Xu, N., 2019, PML and CFS-PML boundary conditions for a mesh-free finite difference solution of the elastic wave equation: Applied Geophysics, **16**(4), P. 438−454.

Virieux J., 1986, P-SV wave propagation in heterogeneous media: Velocity-stress finite-difference method: Geophysics, **51**(4), 889−901.

Wang, S. D., 2003, Acoustic wave equation perfectly matches layer absorption boundary: Oil Geophysical Prospecting, **38**(1), 31−34.

Xing, L., 2006, Absorbing boundary conditions for the numerical simulation of acoustic waves: Journal of Shanghai Second Polytechnic University, **23**(4), 16−22

Yang, H. X., and Wang, H. X., 2013, A study of damping factors in perfectly matched layers for the numerical simulation of seismic waves: Applied Geophysics, **10**(1), P. 63−70.

Yin, W., Yin, X Y, and Wu, G. C., et al, 2006, The method of finite difference high precision elastic wave equations in the frequency domain and wavefield simulation: Chinese Journal of Geophysics (in Chinese), **49**(2), 561−568.

Yuan, W. L., and Liang, C. H., 2000, General optimization of the perfectly matched layers: Journal of China Institute of Communications, **21**(3), 47−51.

Zhang, L. X., Fu, L. Y., and Pei, Z. L., 2010, Finite difference modeling of Biot's poroelastic equations with unsplit convolutional PML and rotated staggered grid: Chinese Journal of Geophysics (in Chinese), **53**(10), 2470−2483.

Appendix A: Conventional SPML boundary

Taking the x-axis as an example, the complex coordinate transformation is (Berenger, 1994)

$$\begin{cases} \partial_{\tilde{x}} = \dfrac{1}{s_x}\dfrac{\partial}{\partial x} \\ s_x = 1 + \dfrac{d_x(x)}{i\omega} \end{cases}, \tag{A-1}$$

where $i = \sqrt{-1}$ represents the damping coefficient that attenuates the transmitted wave.

Substituting equation (A-1) into equation (3), the following is obtained:

$$(i\omega)^2 \rho \hat{u}_x = \begin{pmatrix} (\lambda+2\mu)\left(\dfrac{i\omega}{i\omega+d_x(x)}\right)^2 \dfrac{\partial^2 \hat{u}_x}{\partial x^2} - (\lambda+2\mu)\dfrac{(i\omega)^2 d_x'(x)}{(i\omega+d_x(x))^3}\dfrac{\partial \hat{u}_x}{\partial x} \\ +\mu\left(\dfrac{i\omega}{i\omega+d_z(z)}\right)^2 \dfrac{\partial^2 \hat{u}_x}{\partial z^2} - \mu\dfrac{(i\omega)^2 d_z'(z)}{(i\omega+d_z(z))^3}\dfrac{\partial \hat{u}_x}{\partial z} \\ +(\lambda+\mu)\left(\dfrac{i\omega}{i\omega+d_x(x)}\right)\left(\dfrac{i\omega}{i\omega+d_z(z)}\right)\dfrac{\partial^2 \hat{u}_z}{\partial x \partial z} \end{pmatrix}, \tag{A-2a}$$

$$(i\omega)^2 \rho \hat{u}_z = \begin{pmatrix} \mu\left(\dfrac{i\omega}{i\omega+d_x(x)}\right)^2 \dfrac{\partial^2 \hat{u}_z}{\partial x^2} - \mu\dfrac{(i\omega)^2 d_x'(x)}{(i\omega+d_x(x))^3}\dfrac{\partial \hat{u}_z}{\partial x} \\ +(\lambda+2\mu)\left(\dfrac{i\omega}{i\omega+d_z(z)}\right)^2 \dfrac{\partial^2 \hat{u}_z}{\partial z^2} - (\lambda+2\mu)\dfrac{(i\omega)^2 d_z'(z)}{(i\omega+d_z(z))^3}\dfrac{\partial \hat{u}_z}{\partial z} \\ +(\lambda+\mu)\left(\dfrac{i\omega}{i\omega+d_x(x)}\right)\left(\dfrac{i\omega}{i\omega+d_z(z)}\right)\dfrac{\partial^2 \hat{u}_x}{\partial x \partial z} \end{pmatrix}. \tag{A-2b}$$

We can obtain the time-domain equation by inverse Fourier transform. However, direct inverse Fourier transform will introduce convolution to the time domain, so we usually split the wavefield, taking the x-direction as an example

$$\hat{u}_x = \hat{u}_1 + \hat{u}_2 + \hat{u}_3, \tag{A-3}$$

where $\hat{u}_1$ and $\hat{u}_2$ are the partial derivatives in the x- and z-directions and $\hat{u}_3$ is the partial derivative in the *xz*-direction. Thus, we can decompose equation (A-3) into

$$\begin{cases} \hat{u}_x = \hat{u}_1 + \hat{u}_2 + \hat{u}_3 \\ \rho\left(i\omega + d_x(x)\right)^2 \hat{u}_1 = \left(\lambda + 2\mu\right)\dfrac{\partial^2 \hat{u}_x(x,z,\omega)}{\partial x^2} + P_1(x,z,\omega) \\ \rho\left(i\omega + d_z(z)\right)^2 \hat{u}_2 = \mu\dfrac{\partial^2 \hat{u}_x(x,z,\omega)}{\partial z^2} + P_2(x,z,\omega) \\ \rho\left(i\omega + d_x(x)\right)\left(i\omega + d_z(z)\right)\hat{u}_3 = \left(\lambda + \mu\right)\dfrac{\partial^2 \hat{u}_z(x,z,\omega)}{\partial x \partial z} \\ P_1(x,z,\omega) = -\left(\lambda + 2\mu\right)\dfrac{d_x'(x)}{i\omega + d_x(x)}\dfrac{\partial \hat{u}_x(x,z,\omega)}{\partial x} \\ P_2(x,z,\omega) = -\mu\dfrac{\left(i\omega\right)^2 d_z'(z)}{\left(i\omega + d_z(z)\right)^3}\dfrac{\partial \hat{u}_x(x,z,\omega)}{\partial z} \end{cases}. \tag{A-4}$$

By inverse Fourier transform of the equation, we can obtain the SPML equation in the time domain.

$$\begin{cases} u_x = u_1 + u_2 + u_3 \\ \dfrac{\partial^2 u_1}{\partial t^2} + 2d_x(x)\dfrac{\partial u_1}{\partial t} + d_x^2(x)u_1 = v_p^2(x,z)\dfrac{\partial^2 u_x(x,z,t)}{\partial x^2} + p_1(x,z,t) \\ \dfrac{\partial^2 u_2}{\partial t^2} + 2d_z(z)\dfrac{\partial u_2}{\partial t} + d_z^2(z)u_2 = v_s^2(x,z)\dfrac{\partial^2 u_x(x,z,t)}{\partial z^2} + p_2(x,z,t) \\ \dfrac{\partial^2 u_3}{\partial t^2} + d_x(x)\dfrac{\partial u_3}{\partial t} + d_z(z)\dfrac{\partial u_3}{\partial t} + d_x(x)d_z(z)u_3 = \begin{pmatrix} v_p^2(x,z) \\ -v_s^2(x,z) \end{pmatrix}\dfrac{\partial^2 u_z(x,z,t)}{\partial x \partial z}, \\ \dfrac{\partial p_1(x,z,t)}{\partial t} + d_x(x)p_1(x,z,t) + v_p^2(x,z)d_x'(x)\dfrac{\partial u_x(x,z,t)}{\partial x} = 0 \\ \dfrac{\partial p_1(x,z,t)}{\partial t} + d_z(z)p_2(x,z,t) + v_s^2(x,z)d_z'(z)\dfrac{\partial u_x(x,z,t)}{\partial z} = 0 \end{cases} \tag{A-5}$$

where v_p and v_s represent the P- and S-wave velocities, respectively, with $v_p = \sqrt{\dfrac{\lambda+\mu}{\rho}}$ and $v_s = \sqrt{\dfrac{\mu}{\rho}}$.

Appendix B: Conventional CPML boundary

Different from the conventional SPML boundary, the complex stretching variable of the CPML absorbing boundary in the x-axis is (Komatitsch, 2007)

$$\begin{cases} \partial_{\tilde{x}} = \dfrac{1}{s_x}\dfrac{\partial}{\partial x} \\ s_x = k_x(x) + \dfrac{d_x(x)}{\alpha_x(x) + i\omega} \end{cases}, \tag{B-1}$$

where $i = \sqrt{-1}$, d_x represents the damping profile in the traditional PML that attenuates the transmission wave (Wang, 2003, Yang and Wang, 2013), and α_x and k_x represent the complex frequency shift and the grid compression parameter, respectively. In the PML region, $d_x \geq 0$, $\alpha_x \geq 0$, and $k_x \geq 1$. In the computational domain, $k_x = 1$, and $d_x = 0$. Usually, the parameters in the x-axis are as follows (Li et al., 2010):

$$\begin{cases} k_x = 1 + k_{\max}\left(\dfrac{x - x_0}{d}\right)^{n_1} \\ d_x = d_{\max}\left(\dfrac{x - x_0}{d}\right)^{n_1+n_2} \\ \alpha_x = \alpha_{\max}\left(\dfrac{d - x + x_0}{d}\right)^{n_3} \end{cases}, \tag{B-2}$$

with

$$\begin{aligned} &k_{\max} = 0,\ \alpha_{\max} = 2\pi f_c, \\ &d_{\max} = (1 + n_1 + n_2)c_0 \log(1/R_0)/(2d), \end{aligned} \tag{B-3}$$

where x_0 and d denote the starting position coordinates and thickness of the CPML boundary (here it is 1×10^{-6}) (Festa and Nielsen, 2003) and n_1 and n_2 are the exponential factors of the CPML layer attenuation change and usually take the value that similarly controls the frequency shifting scale, which is usually $n_1 = 2$, $n_2 = 0$, and $n_3 = 1$ (Li et al., 2010, Zhang et al., 2010, Yuan and Liang, 2000, Katsibas and Antonopulos, 2004). The values of k_z, d_z, and α_z are consistent with those of k_x, d_x, and α_x.

The conventional CPML boundary is based on the first-order system. Substituting equation (B-1) into frequency-domain equation:Taking the inverse Fourier transform, we get

$$\begin{cases} \rho\dfrac{\partial^2 u_x}{\partial t^2} = F^{-1}\left(\dfrac{1}{s_x}\right) * \dfrac{\partial \sigma_{xx}}{\partial x} + F^{-1}\left(\dfrac{1}{s_z}\right) * \dfrac{\partial \tau_{xz}}{\partial z} \\ \rho\dfrac{\partial^2 u_z}{\partial t^2} = F^{-1}\left(\dfrac{1}{s_x}\right) * \dfrac{\partial \tau_{xz}}{\partial x} + F^{-1}\left(\dfrac{1}{s_z}\right) * \dfrac{\partial \sigma_{zz}}{\partial z} \\ \sigma_{xx} = \left(\lambda + 2\mu\right)F^{-1}\left(\dfrac{1}{s_x}\right) * \dfrac{\partial u_x}{\partial x} + \lambda F^{-1}\left(\dfrac{1}{s_z}\right) * \dfrac{\partial u_z}{\partial z}{}_x \\ \sigma_{zz} = \left(\lambda + 2\mu\right)F^{-1}\left(\dfrac{1}{s_z}\right) * \dfrac{\partial u_z}{\partial z} + \lambda F^{-1}\left(\dfrac{1}{s_x}\right) * \dfrac{\partial u_x}{\partial x} \\ \tau_{xz} = \mu\left(F^{-1}\left(\dfrac{1}{s_x}\right) * \dfrac{\partial u_z}{\partial x} + F^{-1}\left(\dfrac{1}{s_z}\right) * \dfrac{\partial u_x}{\partial z}\right) \end{cases}, \tag{B-4}$$

where * denotes the convolution. We find

$$F^{-1}\left(\frac{1}{s_x}\right)=\frac{\delta(t)}{k_x(x)}+\varepsilon_x(t), \tag{B-5}$$

Moreover, $\varepsilon_x(t)$ is:

$$\varepsilon_x(t)=-\frac{d_x(x)}{k_x^2(x)}H(t)e^{-(d_x/k_x+\alpha_x)t}, \tag{B-6}$$

where $\delta(t)$ and $H(t)$ denote the Dirac delta and the Heaviside distributions, respectively. We find

$$\frac{\partial^2 u_x}{\partial t^2}=\frac{1}{\rho}\left(\begin{array}{l}\dfrac{1}{k_x(x)}\dfrac{\partial\sigma_{xx}}{\partial x}+\dfrac{A_x}{k_x(x)}\\ +\dfrac{1}{k_z(z)}\dfrac{\partial\tau_{xz}}{\partial z}+\dfrac{B_z}{k_z(z)}\end{array}\right), \tag{B-7}$$

where A_x and B_z are auxiliary variables given by

$$\begin{cases}\dfrac{\partial A_x}{\partial t}=-\delta_x\dfrac{\partial\sigma_{xx}}{\partial x}-\beta_x A_x\\ \dfrac{\partial B_z}{\partial t}=-\delta_z\dfrac{\partial\tau_{xz}}{\partial z}-\beta_z B_z\end{cases}. \tag{B-8}$$

Also, $\delta_x = d_x(x) / k_x(x)$, and $\beta_x = d_x(x)/k_x(x) + \alpha_x(x)$. Finally, we get the CPML equation

$$\begin{cases}\rho\dfrac{\partial^2 u_x}{\partial t^2}=\dfrac{1}{k_x(x)}\dfrac{\partial\sigma_{xx}}{\partial x}+\dfrac{A_x}{k_x(x)}+\dfrac{1}{k_z(z)}\dfrac{\partial\tau_{xz}}{\partial z}+\dfrac{B_z}{k_z(z)}\\ \rho\dfrac{\partial^2 u_x}{\partial t^2}=\dfrac{1}{k_x(x)}\dfrac{\partial\tau_{xz}}{\partial x}+\dfrac{C_x}{k_x(x)}+\dfrac{1}{k_z(z)}\dfrac{\partial\sigma_{zz}}{\partial z}+\dfrac{D_z}{k_z(z)}\\ \sigma_{xx}=\dfrac{(\lambda+2\mu)}{k_x(x)}\dfrac{\partial u_x}{\partial x}+\dfrac{(\lambda+2\mu)}{k_x(x)}E_x+\dfrac{\lambda}{k_z(z)}\dfrac{\partial u_z}{\partial z}+\dfrac{\lambda}{k_z(z)}F_z\\ \sigma_{zz}=\dfrac{(\lambda+2\mu)}{k_z(z)}\dfrac{\partial u_z}{\partial z}+\dfrac{(\lambda+2\mu)}{k_z(z)}F_z+\dfrac{\lambda}{k_x(x)}\dfrac{\partial u_x}{\partial x}+\dfrac{\lambda}{k_x(x)}E_x\\ \tau_{xz}=\dfrac{\mu}{k_x(x)}\dfrac{\partial u_z}{\partial x}+\dfrac{\mu}{k_x(x)}G_x+\dfrac{\mu}{k_z(z)}\dfrac{\partial u_x}{\partial z}+\dfrac{\mu}{k_z(z)}H_z\end{cases}, \tag{B-9}$$

where C_x, D_z, E_x, F_z, G_x, and H_z are similar to A_x and B_z. The equation can be written in second-order form

$$\begin{cases}\rho\dfrac{\partial^2 u_x}{\partial t^2}-(\lambda+2\mu)\dfrac{\partial^2 u_x}{\partial x^2}-\mu\dfrac{\partial^2 u_x}{\partial z^2}-(\lambda+2\mu)\dfrac{\partial^2 u_z}{\partial x\partial z}=f_1\\ \rho\dfrac{\partial^2 u_z}{\partial t^2}-\mu\dfrac{\partial^2 u_z}{\partial x^2}-(\lambda+2\mu)\dfrac{\partial^2 u_z}{\partial z^2}-(\lambda+2\mu)\dfrac{\partial^2 u_x}{\partial x\partial z}=f_2\end{cases}, \tag{B-10}$$

where f_1 and f_2 are as follows:

$$\begin{cases}f_1=\left[\begin{array}{l}-\dfrac{k_x'(x)}{k_x(x)}\dfrac{\partial}{\partial x}\left(\dfrac{(\lambda+2\mu)}{k_x(x)}\dfrac{\partial u_x}{\partial x}+\dfrac{(\lambda+2\mu)}{k_x(x)}E_x+\dfrac{\lambda}{k_z(z)}\dfrac{\partial u_z}{\partial z}+\dfrac{\lambda}{k_z(z)}F_z\right)\\ -\dfrac{k_z'(z)}{k_z(z)}\dfrac{\partial}{\partial z}\left(\dfrac{\mu}{k_x(x)}\dfrac{\partial u_z}{\partial x}+\dfrac{\mu}{k_x(x)}G_x+\dfrac{\mu}{k_z(z)}\dfrac{\partial u_x}{\partial z}+\dfrac{\mu}{k_z(z)}H_z\right)\\ +\dfrac{\partial}{\partial x}\left(\dfrac{k_x'(x)(\lambda+2\mu)}{k_x(x)}\dfrac{\partial u_x}{\partial x}+\dfrac{(\lambda+2\mu)}{k_x(x)}E_x+\dfrac{k_z'(z)\lambda}{k_z(z)}\dfrac{\partial u_z}{\partial z}+\dfrac{\lambda}{k_z(z)}F\right)\\ +\dfrac{\partial}{\partial z}\left(\dfrac{k_x'(x)(\lambda+2\mu)}{k_x(x)}\dfrac{\partial u_x}{\partial x}+\dfrac{(\lambda+2\mu)}{k_x(x)}E_x+\dfrac{k_z'(z)\lambda}{k_z(z)}\dfrac{\partial u_z}{\partial z}+\dfrac{\lambda}{k_z(z)}F\right)\\ -\dfrac{A_x}{k_x(x)}-\dfrac{B_z}{k_z(z)}\end{array}\right]\\ f_2=\left[\begin{array}{l}-\dfrac{k_x'(x)}{k_x(x)}\dfrac{\partial}{\partial x}\left(\dfrac{\mu}{k_x(x)}\dfrac{\partial u_z}{\partial x}+\dfrac{\mu}{k_x(x)}G_x+\dfrac{\mu}{k_z(z)}\dfrac{\partial u_x}{\partial z}+\dfrac{\mu}{k_z(z)}H_z\right)\\ -\dfrac{k_z'(z)}{k_z(z)}\dfrac{\partial}{\partial z}\left(\dfrac{(\lambda+2\mu)}{k_z(z)}\dfrac{\partial u_z}{\partial z}+\dfrac{(\lambda+2\mu)}{k_z(z)}F_z+\dfrac{\lambda}{k_x(x)}\dfrac{\partial u_x}{\partial x}+\dfrac{\lambda}{k_x(x)}E_x\right)\\ +\dfrac{\partial}{\partial x}\left(\dfrac{k_x'(x)\mu}{k_x(x)}\dfrac{\partial u_z}{\partial x}+\dfrac{\mu}{k_x(x)}G_x+\dfrac{k_z'(z)\mu}{k_z(z)}\dfrac{\partial u_x}{\partial z}+\dfrac{\mu}{k_z(z)}H_z\right)\\ +\dfrac{\partial}{\partial z}\left(\dfrac{k_z'(z)(\lambda+2\mu)}{k_z(z)}\dfrac{\partial u_z}{\partial z}+\dfrac{(\lambda+2\mu)}{k_z(z)}F_z+\dfrac{k_x'(x)\lambda}{k_x(x)}\dfrac{\partial u_x}{\partial x}+\dfrac{\lambda}{k_x(x)}E_x\right)\\ -\dfrac{C_x}{k_x(x)}-\dfrac{D_z}{k_z(z)}\end{array}\right]\end{cases}, \tag{B-11}$$

with $k_x'(x) = k_x(x) - 1$.

Yang Ling-Yun, graduated from China University of Petroleum (East China) in 2021 and obtained his master's degree. Now he is a Ph.D. student at the same university. His main research interests are seismic wave propagation, forward modeling, and inversion.

Email: 1477052477@qq.com

Corresponding author

Wu Guo-Chen received his Ph.D. (2006) degree in solid geophysics from Tongji University. Now he is a professor at China University of Petroleum (East China) and works on teaching and research of seismic waves theory, seismic inversion, and reservoir prediction.

Email: guochenwu@upc.edu.cn